

Thin film solar cells based on the heterojunction of colloidal PbS quantum dots with CdS

Khagendra P. Bhandari^{a,*}, Paul J. Roland^a, Hasitha Mahabaduge^a, Neale O. Haugen^a, Corey R. Grice^a, Sohee Jeong^c, Tienneke Dykstra^a, Jianbo Gao^{a,b,*}, Randy J. Ellingson^{a,*}

^a Wright Center for Photovoltaic Innovation and Commercialization, Department of Physics and Astronomy, The University of Toledo, 2801 W. Bancroft Street, Toledo, OH 43606, USA

^b National Renewable Energy Laboratory (NREL), 16253 Denver West Parkway, Golden, CO 80401, USA

^c Nanomechanical Research Division, Korea Institute of Machinery and Materials, Daejeon 305-343, Republic of Korea

ARTICLE INFO

Article history:

Received 25 January 2013

Received in revised form

9 July 2013

Accepted 12 July 2013

Keywords:

Quantum dot

PbS

CdS

Solar cell

Thin film

ABSTRACT

Here we report on heterojunction PbS quantum dot (QD) solar cells using RF magnetron sputtered CdS as the n-type window layer. These solar cells generate large open circuit voltage compared to previously reported PbS-QD solar cells. Our investigations of this device design show an optimized CdS film thickness of 70 nm and an optimized PbS QD diameter of ~2.7 nm, corresponding to a bandgap energy of ~1.57 eV. Under simulated AM1.5 G illumination, we attain short circuit current as high as 12 mA-cm⁻², an open circuit voltage of 0.65 V and efficiency as high as 3.3%.

© 2013 Elsevier B.V. All rights reserved.

1. Introduction

Researchers have been investigating suitable n-type heteropartners for PbS quantum dot (QD) solar cells for several years. To date, only ZnO and TiO₂ in their various forms (nanoparticles, nanowires, and bulk thin film) have been widely used as n-type heteropartners for PbS QDs solar cells. With these heteropartners, QD solar cells have shown promising efficiencies in the 4–7% range up to 7.4% [1,2]. ZnO is a wide bandgap (3.37 eV) II–VI semiconductor, and typically shows n-type character even in the absence of intentional doping with low carrier concentration. The synthesis of nanocrystalline (NC) TiO₂ paste for industrial production involves a lengthy process which may be economically challenging, [3] and because of its relatively small electron affinity, TiO₂ cannot be utilized for all sized PbS QDs (efficient electron transfer from PbS QDs to TiO₂ occurs only for QD diameters below approximately 4.3 nm) [4]. These facts, together with the desire to expand our knowledge of photovoltaic (PV) materials science,

suggest consideration of other possible heteropartners for the PbS QDs solar cells.

In this study we have explored sputtered CdS as a heteropartner for PbS QD solar cells for comparison with ZnO and nanostructure TiO₂. CdS is a non-stoichiometric n-type semiconductor with a direct band gap energy of 2.42 eV [5]. We report here on CdS/PbS-QD heterojunction solar cells that show an open circuit voltage as high as ~0.65 V. To our knowledge, no previous report has been made on photovoltaic devices based on RF magnetron sputtered CdS as a window layer for a PbS QD thin film absorber layer [6].

Thin films of CdS have been studied extensively over the past three decades, owing in large part to the fact that CdS has been the most widely used and most successful n-type window layer for high efficiency thin film solar cells based on CdTe [7,8] and Cu (InGa)Se₂ (CIGS) [9,10]. Various techniques such as chemical vapor deposition [11], RF magnetron sputtering [12], and chemical bath deposition [13] have been used to make uniform and transparent CdS films to produce high efficiency solar cells. For CdS, sputtered films have shown both larger crystalline grain size as well as smoother surface roughness as compared with films produced by chemical bath deposition [14]; in addition, we find excellent adhesion qualities for the sputtered CdS films. Sputtering offers

* Corresponding authors at: Wright Center for Photovoltaic Innovation and Commercialization, Department of Physics and Astronomy, The University of Toledo, 2801 W. Bancroft Street, Toledo, OH 43606, USA. Tel.: +1 4195303874.

E-mail address: randy.ellingson@utoledo.edu (R.J. Ellingson).

potential benefits in terms of deposition rate, substrate throughput, and film thickness uniformity.

2. Experimental

2.1. Materials

All chemicals, oleic acid (OA), octadecene (ODE, > 95%), hexamethyldisilane-thiane ((TMS)₂S), lead(II) oxide (PbO, 99.9+%), ethyl alcohol (EtOH, absolute, anhydrous), acetonitrile (99.8% anhydrous), hexane (C₆H₁₄, anhydrous, 95.0%), and 1,2-ethanedithiol (98.0%), were purchased from Sigma-Aldrich except EtOH and OA, which were obtained from Fisher Scientific.

2.2. PbS QD synthesis

The synthesis of PbS QDs is based on the slightly modified version of Hines and Scholes [15] and is carried out under an inert atmosphere using standard Schlenk line techniques. In a typical synthesis, for example to synthesize ~2.9 nm diameter QDs: 2 mmol of PbO, 10 g of ODE, and 1.14 g of OA are heated to 120–122 °C under N₂ in a 100 mL round bottom three neck flask. The mixture is continuously stirred with a magnetic stirrer. The mixture is heated until all the PbO is dissolved completely typically within 45 min.

In the glove box, 1 mmol (TMS)₂S is dissolved in 3.16 g of nitrogen-purged ODE. The mixture is loaded in a syringe with a needle. The heating mantle is removed and the mixture is injected immediately at 110 °C into a three neck flask. When the temperature of the mixture reaches room temperature, purification is done in air by adding ~5 mL of hexane and ~30 mL of EtOH and centrifuging at 5000 rpm for about 20 min. The supernatant is removed and sediment is cleaned two more times with hexane/

ethanol. QDs so obtained are dried under nitrogen and utilized for the experimental purposes.

2.3. PbS QD solar cell fabrication

PbS-QD film (absorbing layer) fabrication was completed using the layer-by-layer (LbL) deposition method reported elsewhere [16,17]. Patterned indium tin oxide (ITO) coated glass substrates, obtained from Thin Film Devices, Inc., were cleaned by sonication using micro-90[®] (concentrated cleaning solution) and deionized water. Cleaned glass substrates were then dipped into a beaker containing 15–20 mL of QD solution with the concentration of about 8 mg/mL prepared in hexane in a 30 mL beaker followed by a second beaker containing 1 mM EDT solution in acetonitrile. Approximately 20 to 40 dip cycles resulted in QD films of 150–200 nm thickness. Dip-coating was performed either by hand or using a dip coater from NIMA Technology, England. The added thickness of the QD film from each cycle depends on the concentration of the colloidal solution and the removal speed (typically ~0.7 mm/s) of the substrate from the solution. For heterojunction solar cells, CdS was used as the window layer (n-type semiconductor) and was deposited by RF magnetron sputtering in an Ar atmosphere. Prior to deposition of CdS, the chamber was heated to 270 °C for 30 min. The transparent and conducting ITO layer shows a sheet resistance of 32 Ω/□ and forms the top contact of the device. A 150 nm thick gold (Au) film is used as the bottom contact and is deposited either by electron beam evaporation or thermal evaporation methods. Au was selected as the back contact, due to its high work function, to minimize back junction effects [1,18]. Six cells were fabricated on a single substrate, each with an active area of 0.0975 cm².

2.4. PbS QD solution, film, and device characterization

Absorbance spectra (optical density, OD) were measured using a Perkin-Elmer, Lambda 1050, UV/VIS/NIR spectrophotometer.

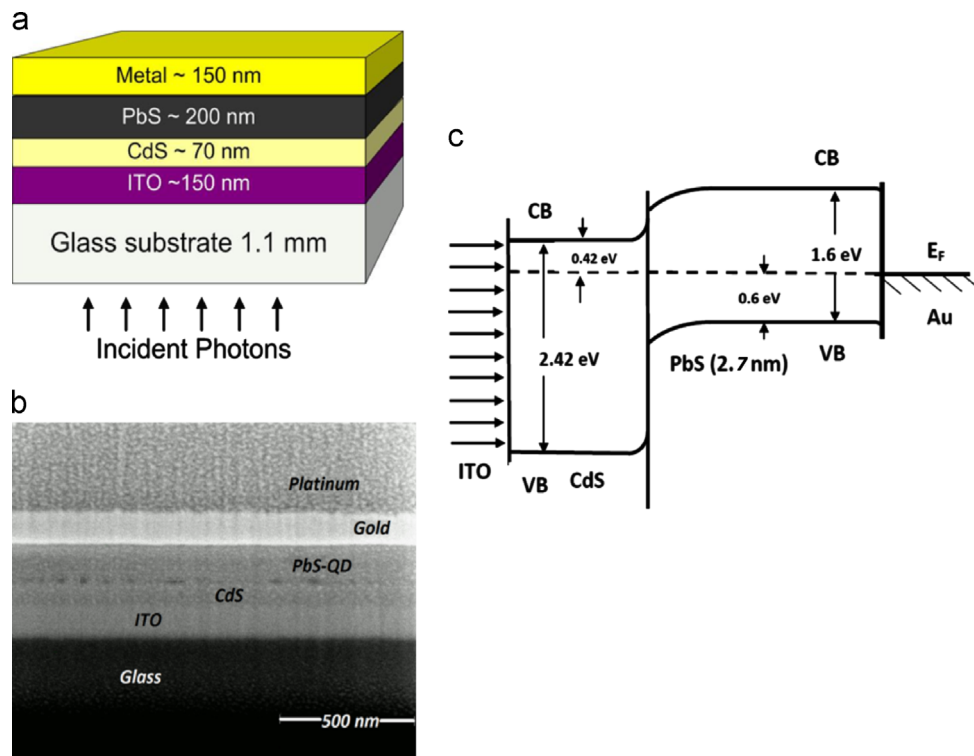


Fig. 1. (a) Schematic of the PbS QD/CdS heterojunction solar cell. (b) Cross-sectional scanning electron microscopy (SEM) of the PbS QD/CdS junction solar cell illustrated in (a). (c) Schematic of the energy band diagram of an ITO/CdS/PbS-QD/Au solar cell.

Photoluminescence spectra (PL) were measured using Fourier Transform Photoluminescence Spectroscopy (FT-PL). Instrumental set up of FT-PL is very similar to the one explained by McDonald et al. [19]. Current–voltage measurements were done with a Keithley 2440 Source-Measure Unit under illumination from an Oriel 91195A-1000 solar simulator, and external quantum efficiency (EQE) measurements were acquired using a PV Measurements Inc., Model IVQE8-C QE system. X-ray diffraction (XRD) spectra were obtained using a Dragon/PXRD; surface roughness for the CdS and PbS-QD films were determined by AFM using a Veeco D3300 V.

3. Results and discussion

Fig. 1 shows the complete solar cell device structure, its cross-sectional view, and equilibrium band diagram. Varying the thicknesses of both the n- and p- type layers, we found the best cell performance using 70 nm of CdS and 150–200 nm of PbS QDs. The completed device was processed for cross-sectional imaging using focused ion beam (FIB) milling, and imaged by scanning electron microscopy (SEM). A layer of platinum was deposited onto the Au layer to avoid Ga⁺ ion implantation and milling of the Au surface during FIB processing [20].

The X-ray diffraction pattern of CdS thin films (see Supporting Information, Fig. S1) deposited at a sputter power of 50 W showed a most prominent diffraction peak at $2\theta = 26.48^\circ$, corresponding to the (002) lattice plane of CdS. The (002) peak, as well as several other peaks arising from (100), (002), (101), (110), (103), (200), (112), (201) and (004) lattice planes, represent the hexagonal wurtzite crystalline phase with inter-plane spacing of 5.83 Å [21,22]. Scherrer analysis of the primary diffraction peak (002) indicates that the film consists of oriented grains with an average size of 33 nm. The optical transmittance of the CdS film was measured for the wavelength range 350–2000 nm (Fig. S2). A 70 nm thick CdS film transmits at >60% for incident light of wavelength longer than 515 nm.

In order to construct the solar cell's band diagram, we investigated the electronic and interface properties of sputtered CdS and PbS-QD thin films. Work functions of CdS films and PbS-QDs were measured by Kelvin probe (KP) and ultraviolet photoelectron spectroscopy (UPS). Work functions of these thin films measured by KP were 4.4 eV (CdS) and 4.5 eV (PbS-QD films). Similarly, the work functions derived by UPS measurements were 4.5 eV (CdS) and 4.9 eV (PbS-QD films). UPS was also used to calculate the valence band maximum (VBM) for both CdS and PbS-QD films. The VBM obtained with respect to the Fermi level, which is considered as the zero binding energy in the UPS spectrum, were 2.0 eV (CdS) and 0.6 eV (PbS-QD films) (Fig. S3). Liu et al. [23] found the work function of CdS to be 4.7 eV and the VBM to be 2.2 eV using a similar method. The band offset at the interface is one of the most important properties for a semiconductor heterostructure device, and enables the design and optimization of different contacts to minimize the loss of photogenerated carriers resulting in a cell with higher conversion efficiency. X-ray photoelectron spectroscopy (XPS) and UPS were used to determine the valence band offset ΔE_V and conduction band offset ΔE_C at the CdS/PbS-QD heterojunction. As discussed in the Supporting Information, the valence band offset between CdS and PbS-QD was found to be 1.4 eV, and the deduced conduction band offset was determined to be 0.57 eV for a PbS-QD of size ~2.7 nm. The carrier concentrations of the bulk CdS and PbS-QD films were determined using capacitance–voltage testing methods and Mott–Schottky analysis as discussed in Supporting Information.

Under illumination, electron–hole pairs photo-generated within the depletion region are separated by the built-in electric field with electrons drifting to the CdS and holes drifting to the PbS-QD layer. When the device terminals are shorted, excess electrons in the CdS

flow through the external circuit to recombine with the excess holes in the PbS QDs side—this represents the photocurrent. The current–voltage (*I*–*V*) characteristics of our best device is shown in Fig. 2. To complete this device, we deposited a 70 nm thick CdS film followed by a PbS-QD film (QD diameter of ~2.7 nm, first exciton peak at ~792 nm, or 1.57 eV) of approximately 200 nm thickness (Fig. S4 presents absorbance and photoluminescence spectra). This solar cell exhibited an open circuit voltage, V_{OC} of 638 mV, short circuit current, J_{SC} of 12.0 mA·cm⁻², and overall photo-conversion efficiency (PCE) of 3.3% when illuminated with 100 mW·cm⁻² simulated AM1.5 G.

We can compare these results with heterojunction devices based on other partner materials such as CdS, ZnO, Bi₂S₃, and TiO₂. Hernandez–Borja reported a study of CdS/PbS solar cells which were not based on quantum dot PbS. Their devices were fabricated using chemical bath deposition, and achieved an efficiency of ~1.6%. The J_{SC} value of 14 mA·cm⁻² and V_{OC} value of 290 mV make sense in that the bandgap energy of bulk PbS is just ~0.4 eV and therefore their device absorbs a much larger portion of the solar spectrum [24]. In a report by Gao et al., solar cells utilizing 1.6 eV band gap PbS QDs and NC ZnO achieved V_{OC} , J_{SC} and PCE values of <600 mV, <5.0 mA·cm⁻² and <2.0% respectively [18]. Choi et al. constructed a solution processed tandem solar cell with NC ZnO as a heteropartner within each of two junctions formed using PbS-QD thin films of 1.0 eV and 1.6 eV band gap energies [25]. The best PbS-QD tandem solar cell attained a V_{OC} of 0.91 V, though the J_{SC} , FF, and PCE were all lower than we report here. Luther et al. constructed a 3% efficient bilayer PbS/ZnO QD heterojunction solar cell using air-stable 1.3 eV PbS QDs [26]. Comparing their results to ours at similar QD bandgap energy, their FF is larger than we obtain, resulting in a larger PCE at similar J_{SC} and V_{OC} values. Recently, Brown et al. demonstrated improvements in PCE for ZnO/PbS-QD heterojunction device through the incorporation of a MoO₃ interlayer between the PbS QD layer and the back contact [27]. They achieved an efficiency of 3.5% from QDs having an effective bandgap of 1.3 eV and using gold as a back contact. For larger dots their devices show slightly better performance than what we have achieved at the same dot size. Employing 3.5 nm diameter PbS QDs and an approach similar to that of Brown et al., Gao et al. fabricated NC ZnO/PbS-QD solar cells showing 4.4% PCE with a J_{SC} of 18 mA cm⁻², which was at the time the certified record QD device efficiency [1]. Rath et al. [28] employed Bi₂S₃ nanocrystals as an n-type semiconductor in their p–n junction based solar cell based on p-type PbS-QD. Their best

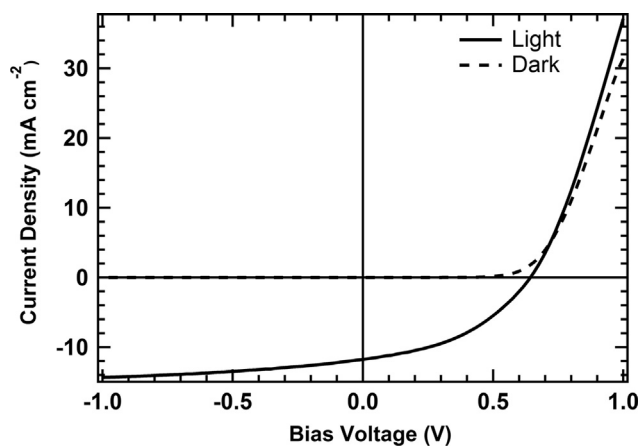


Fig. 2. Current–voltage (*I*–*V*) characteristics of a CdS/PbS-QD heterojunction solar cell recorded in the dark and under 100 mW·cm⁻² simulated AM1.5 illumination. The device was assembled using ~200 nm thick EDT treated PbS-QD film deposited from ~2.7 nm diameter QDs, ~70 nm thick CdS film and gold contact. V_{OC} , J_{SC} , FF and PCE of this cell were 638 mV, 12.0 mA·cm⁻², 43.5% and 3.3% respectively.

device demonstrated V_{OC} 0.44 V, with a power conversion efficiency of 1.6% for 860 nm (1.4 eV bandgap energy) PbS-QDs and over 1% for 1300 nm (0.95 eV) PbS-QDs. Several other reports of PbS QD solar cells exist with PCE results in the 3–5% range [29,30]. Recently, a record QD thin film solar cell efficiency was reported by Ip et al. based on a hybrid passivated PbS QD layer deposited onto a ZnO/TiO₂-coated substrate [2]. Ip et al. achieved a remarkable PCE of 7%, suggesting that further improvements lie ahead for the field. Subsequent to submission of our manuscript, Chang et al. reported results similar to ours employing chemical-bath-deposited CdS as the window layer for their PbS-QD device and achieving comparable efficiency of 3.5% [31].

Experimental and theoretical maximum (modeled) external quantum efficiency (EQE) for the solar cell from Fig. 2 is shown in Fig. 3.

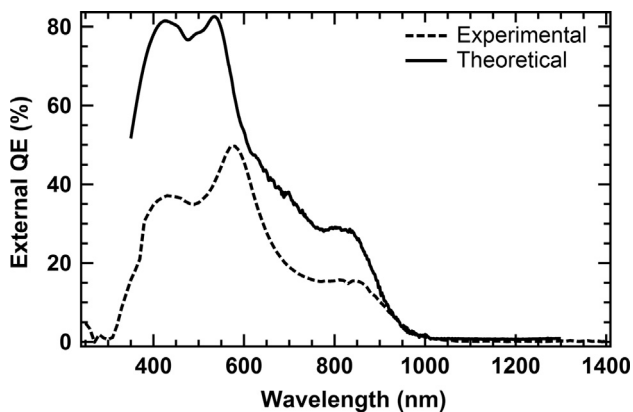


Fig. 3. External quantum efficiency spectrum of the PbS-QD solar cell featured in Fig. 2 from both theoretically and experimentally obtained data. In the theoretical curve, charge collection contribution from both CdS and PbS-QD layers are considered and recombination losses are neglected.

First, the complex refractive index, $\tilde{n}(\lambda) = n(\lambda) + ik(\lambda)$, for the materials used were obtained by spectroscopic ellipsometry (SE). Afterwards, the electric field strength and photo-induced carrier generation rates were calculated as functions of wavelength and position in the film stack following the method outlined by Petterson et al [32]. Specifically, we apply an optical model based on a 2×2 system transfer matrix [32] to model the QE and current losses of our solar cell devices shown in Fig. 1(a). Finally, the EQE curve shown in Fig. 3 was calculated by summing the photons absorbed within the CdS and PbS-QD layers, assuming one electron–hole pair per absorbed photon. While including recombination can in principle yield more detailed performance modeling, specific recombination considerations are excluded as the QD film electronic properties are not yet fully understood. The result shown in Fig. 3 is a prediction of the maximum EQE curve attainable with the given solar cell structure.

The photocurrent generated between 515 and 900 nm is attributable to absorption in the PbS-QDs absorber layer followed by electron transfer to the CdS window layer. The small peak in EQE near 450 nm in Fig. 3 represents photocurrent contributed by the CdS film, which absorbs strongly for photon energies above the bandgap of ~ 2.4 eV (515 nm). Unlike CdTe/CdS thin film solar cells, our data shows contributions from carriers photogenerated in the thin CdS window layer. However, light absorption within the CdS at wavelengths below ~ 512 nm do show a relatively poor EQE of $\sim 35\%$; such losses do not occur within ZnO films which exhibit a bandgap energy close to 3.37 eV and therefore show better transparency in this spectral region.

Our optical model shows that we could improve collection by reducing reflectance at 550 nm and in the near infrared region (NIR) of the spectrum (Fig. S5). This model was also used to calculate the electric field strength and charge carrier generation rate as a function of the depth and wavelength [33]. Our model shows that the CdS absorbs light relatively uniformly from 410 nm to 540 nm (Fig. S6). The QE curve in the 400–540 nm region can be represented as a contribution from both layers (Figs. S7 and S8). It

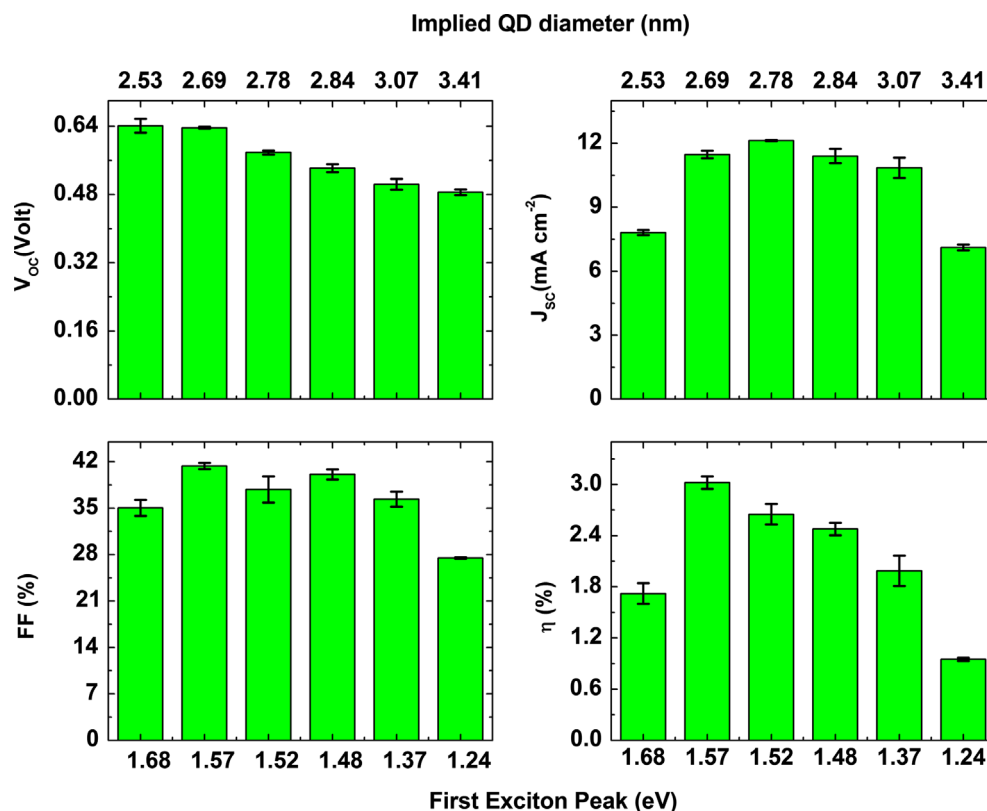


Fig. 4. Dependence of V_{OC} , J_{SC} , FF and PCE on the diameter and effective band gap energy (the first exciton peak, E_g in eV) of PbS-QDs. All solar cell devices were assembled using ~ 200 nm thick EDT-capped PbS-QD film deposited onto ~ 70 nm thick CdS. Diameters of the QDs are based on the first exciton peak values as measured in solution [34, 35].

is clear from Fig. 3 that a large portion of loss occurs due to poor carrier collection and weak photon absorption in the NIR portion of the spectrum.

The performance of our solar cells can be tuned by changing the QD size and hence the electronic energy levels within the QDs. Fig. 4 shows the variation of V_{OC} , J_{SC} , FF and PCE for solar cells assembled using different size QDs as a function of the first exciton peak (effective band gap energy, E_g) of the QDs in eV. Six devices were fabricated at a time and reproduced three times. As each prepared substrate consists of six cells, each column in Fig. 4 is the average of six cells with the error bar representing the standard deviation. We see that V_{OC} decreases with decreasing bandgap (increasing QD size and decreasing quantum confinement). As expected, V_{OC} depends on the valence band and conduction band (HOMO and LUMO) levels of the QDs and is strongly correlated with the size of the QDs.

J_{SC} decreases for both smaller and larger size QDs. For smaller QD diameters (large bandgap), the long wavelength absorption cut-off moves to shorter wavelength, reducing the portion of the spectrum absorbed within the PbS-QD layer, resulting in a decrease in J_{SC} . Larger dots (smaller bandgap) allow larger portions of the solar spectrum to be absorbed by the PbS-QD layer but the driving force for electron transport to the CdS is reduced because of the resulting band alignment. Therefore, judicious selection of the QD size is necessary to achieve optimal J_{SC} . The fill factor shows a similar trend as that of J_{SC} while photo-conversion efficiency demonstrates a maximum for PbS-QDs of diameter ~ 2.7 nm corresponding to the first exciton peak at 792 nm.

The variation of V_{OC} , J_{SC} , FF and PCE for solar cells assembled using PbS-QDs of size ~ 2.78 nm corresponds to the first exciton peak at 816 nm, with respect to CdS film thickness shown in Fig. 5. Since the thin PbS-QD film (~ 200 nm) is deposited on top of CdS by a solution based method, surface roughness of the CdS film (Fig. S9) may hinder uniform deposition of the QD film. It is found that surface roughness of the PbS-QD film (Fig. S10) is larger when deposited onto thicker CdS films. This rough surface may yield a higher density of trap centers on the QD film surface, increasing

the reverse saturation current density (J_0). One clear effect of defect-related recombination is a reduction in the open circuit voltage (V_{OC}), which depends not only on J_0 but also on the photo-generated current density (J_{ph}) of the solar cell by the relation

$$V_{oc} = \frac{nKT}{e} \ln \left(\frac{J_{ph}}{J_0} + 1 \right) \quad (1)$$

where n is the ideality factor, K is the Boltzmann constant, T is the absolute temperature, and e the charge of an electron. J_0 depends on the recombination in the solar cell and may vary by orders of magnitude. Hence, V_{OC} is one measure of recombination in the device for the thicker CdS layers as shown in Fig. 5. In our case, V_{OC} decreases as the CdS thickness increases from 35 nm to 150 nm. However, for CdS/CdTe solar cells the V_{OC} dependence on CdS thickness follows an opposite trend. Plotnikov et al.[36] studied the V_{OC} dependence on CdS thickness for the cells deposited on bare TEC-15 and HRT-coated TEC-15 substrates and found higher V_{OC} for higher CdS film thickness until it became maximum for about 130 nm CdS film. However, they were able to make high performance CdS/CdTe devices when the CdS film thickness was about 80 nm on bare TEC-15 and 30–130 nm on HRT TEC-15.

In most of the devices we fabricated with CdS thickness of 70 nm, higher J_{SC} and ultimately higher efficiencies were observed. The EQE (Fig. 3) shows an apparent contribution of the CdS to the photocurrent, especially in the higher energy region. This contribution is found to be maximized when CdS thickness is 70 nm, indicating an optimum thickness of the window layer at 70 nm. With increasing photon energy above the band gap of 2.42 eV, CdS shows an increasing absorption coefficient. Within CdS, the penetration depth for 2.48 eV (500 nm) photons is ~ 62 nm. As the CdS layer thickness is increased, the absorption within CdS of higher energy photons reduces the photon flux absorbed within the PbS-QD layer, and this may in part explain the observed drop in J_{SC} . The FF is lower for the two thickest CdS films, in accordance with higher series resistance and lower shunt resistance (Fig. S11). A high series resistance reduces J_{SC} and contributes to a reduced FF. A low shunt resistance reduces V_{OC} under load

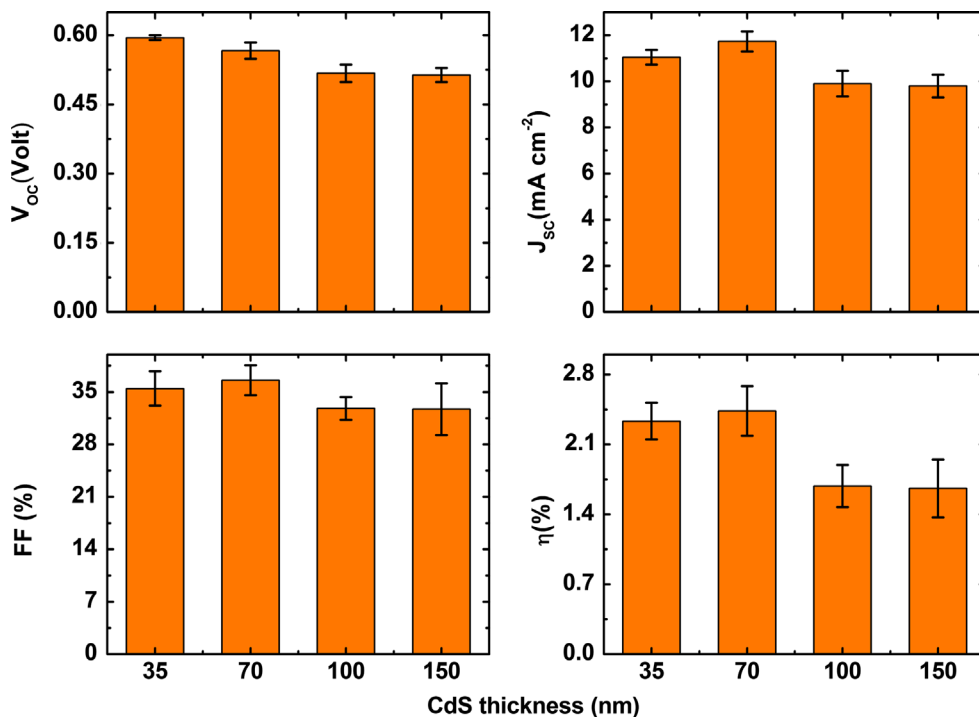


Fig. 5. Dependence on window layer thickness of the performance of PbS-QDs solar cells. Six devices for each CdS thickness (35, 70, 100 and 150 nm) were fabricated on a single substrate by depositing a PbS-QD film of thickness ~ 200 nm. The PbS QD diameter used in these studies was ~ 2.78 nm, corresponding to the first exciton peak at 816 nm (1.52 eV).

and also lowers the FF. Because of the bulky organic molecules in QDs, mobility of the charge carriers is low [37], R_s values are higher, and R_{sh} values are smaller than they appear in commercial thin film solar cells. The series and shunt resistances of our best device are $21 \Omega \text{ cm}^2$ and $204 \Omega \text{ cm}^2$ respectively. Series and shunt resistances of CdS/CdTe solar cells of device area of 0.08 cm^2 obtained by Vigil et al. [38] were $2.9 \Omega \text{ cm}^2$ and $787 \Omega \text{ cm}^2$ when S/Cd ratio was 5/1. The highest efficiency they achieved from this device is 12.3%. Similarly, from a device area of 0.25 cm^2 , Pena et al. [39] obtained series and shunt resistances $8.0 \Omega \text{ cm}^2$ and $631 \Omega \text{ cm}^2$ from CdS/CdTe solar cells of efficiency 6.3% with Cu/Mo back contact.

We studied the stability of the devices by measuring their J - V characteristics with respect to time following a similar procedure as Tang et al. [40] For these measurements, two identical devices were used, keeping one of the devices in ambient atmosphere and another in an inert N_2 atmosphere. Our two month long study shows no significant differences between storage in ambient air and storage in an inert atmosphere as shown in Fig. S12. This indicates that the performance of these devices does not degrade significantly in air on the timescale of months, though longer time studies are required to determine the extent of the air-stability of these devices.

4. Conclusions

We report the first heterojunction solar cells based on PbS-QDs and RF magnetron sputtered CdS thin films, demonstrating an achieved efficiency of 3.3%. Our devices exhibited high V_{oc} values when compared to Schottky junction solar cells and other PbS-QDs heterojunction solar cells. We find that PbS-QDs with the first exciton peak near 800 nm yielded the best devices. Similarly, CdS thin films with thicknesses of $\sim 70 \text{ nm}$ are considered as an optimized window layer thickness for the CdS/PbS-QD combination. From this study, we conclude that understanding and optimizing the quality of the PbS coupled QD film, as well as the properties of the interface between the CdS and the PbS-QD film, are both essential to enhance the performance of heterojunction QD thin film solar cells in the future.

Acknowledgments

The authors would like to thank Y. Xie for his assistance to measure surface roughness using atomic force microscopy. K. Bhandari, T. Dykstra, R. Ellingson, N. Haugen, and P. Roland received support from the Air Force Research Laboratory under Contracts FA9453-08-C-0172 and FA9453-11-C-0253; CG was supported by the University of Toledo's School for Solar and Advanced Renewable Energy; K. Bhandari and J. Gao received support from the National Renewable Energy Laboratory Seed Fund program; R. Ellingson received support from the State of Ohio Wright Centers program; and S. Jeong was supported by the Global Frontier R&D Program by the Center for Multiscale Energy Systems.

Appendix A. Supporting information

Supplementary data associated with this article can be found in the online version at <http://dx.doi.org/10.1016/j.solmat.2013.07.018>.

References

- [1] J. Gao, C.L. Perkins, J.M. Luther, M.C. Hanna, H.-Y. Chen, O.E. Semonin, A. J. Nozik, R.J. Ellingson, M.C. Beard, n-Type transition metal oxide as a hole extraction layer in PbS quantum dot solar cells, *Nano Letters* 11 (2011) 3263–3266.
- [2] A.H. Ip, S.M. Thon, S. Hoogland, O. Voznyy, D. Zhitomirsky, R. Debnath, L. Levina, L.R. Rollny, G.H. Carey, A. Fischer, K.W. Kemp, I.J. Kramer, Z. Ning, A.J. Labelle, K.W. Chou, A. Amassian, E.H. Sargent, Hybrid passivated colloidal quantum dot solids, *Nat Nano* 7 (2012) 577–582.
- [3] S. Ito, P. Chen, P. Comte, M.K. Nazeeruddin, P. Liska, P. Péchy, M. Grätzel, Fabrication of screen-printing pastes from TiO_2 powders for dye-sensitized solar cells, *Progress in Photovoltaics: Research and Applications* 15 (2007) 603–612.
- [4] B.-R. Hyun, Y.-W. Zhong, A.C. Bartnik, L. Sun, H.D. Abruña, F.W. Wise, J. D. Goodreau, J.R. Matthews, T.M. Leslie, N.F. Borrelli, Electron injection from colloidal PbS quantum dots into titanium dioxide nanoparticles, *ACS Nano* 2 (2008) 2206–2212.
- [5] D. Lincot, G. Hodes, Chemical Solution Deposition of Semiconducting and Non-Metallic Films: Proceedings of the International Symposium, Electrochemical Society, 2006.
- [6] Subsequent to the submission of our manuscript, the work by Chang et al. (Ref. #31) reported a study of all-solution-processed CdS/PbS solar cells in which the CdS thin film was prepared using chemical bath deposition. The study achieved similar results for reported device efficiency.
- [7] N. Romeo, A. Bosio, R. Tedeschi, A. Romeo, V. Canevari, A highly efficient and stable CdTe/CdS thin film solar cell, *Solar Energy Materials and Solar Cells* 58 (1999) 209–218.
- [8] K.D. Dobson, I. Visoly-Fisher, G. Hodes, D. Cahen, Stability of CdTe/CdS thin-film solar cells, *Solar Energy Materials and Solar Cells* 62 (2000) 295–325.
- [9] K. Ramanathan, M.A. Contreras, C.L. Perkins, S. Asher, F.S. Hasoon, J. Keane, D. Young, M. Romero, W. Metzger, R. Noufi, J. Ward, A. Duda, Properties of 19.2% efficiency ZnO/CdS/CuInGaSe2 thin-film solar cells, *Progress in Photovoltaics: Research and Applications* 11 (2003) 225–230.
- [10] R. Scheer, H.W. Schock, Chalcogenide Photovoltaics: Physics, Technologies, and Thin Film Devices, John Wiley & Sons, 2011.
- [11] H. Uda, H. Yonezawa, Y. Ohtsubo, M. Kosaka, H. Sonomura, Thin CdS films prepared by metalorganic chemical vapor deposition, *Solar Energy Materials and Solar Cells* 75 (2003) 219–226.
- [12] J.-H. Lee, D.-J. Lee, Effects of CdCl_2 treatment on the properties of CdS films prepared by r.f. magnetron sputtering, *Thin Solid Films* 515 (2007) 6055–6059.
- [13] J.Y. Choi, K.-J. Kim, J.-B. Yoo, D. Kim, Properties of cadmium sulfide thin films deposited by chemical bath deposition with ultrasonication, *Solar Energy* 64 (1998) 41–47.
- [14] S.L. Wang, X.J. Wang, W.Z. Wang, C.J. Liang, Z. Wang, Z. Qi, Comparative study on thin films of cadmium sulfide prepared by chemical bath deposition and radio frequency magnetron sputtering, *Guang Pu Xue Yu Guang Pu Fen Xi* 32 (2012) 1094–1097.
- [15] M.A. Hines, G.D. Scholes, Colloidal PbS nanocrystals with size-tunable near-infrared emission: observation of post-synthesis self-narrowing of the particle size distribution, *Advanced Materials* 15 (2003) 1844–1849.
- [16] J.M. Luther, M. Law, M.C. Beard, Q. Song, M.O. Reese, R.J. Ellingson, A.J. Nozik, Schottky Solar Cells, Based on Colloidal Nanocrystal Films, *Nano Letters* 8 (2008) 3488–3492.
- [17] J. Tang, X. Wang, L. Brzozowski, D.A.R. Barkhouse, R. Debnath, L. Levina, E. H. Sargent, Schottky quantum dot solar cells stable in air under solar illumination, *Advanced Materials* 22 (2010) 1398–1402.
- [18] J. Gao, J.M. Luther, O.E. Semonin, R.J. Ellingson, A.J. Nozik, M.C. Beard, Quantum dot size dependent J - V characteristics in heterojunction ZnO/PbS quantum dot solar cells, *Nano Letters* 11 (2011) 1002–1008.
- [19] T.J. McDonald, Near-infrared Fourier transform photoluminescence spectrometer with tunable excitation for the study of single-walled carbon nanotubes, *Rev. Sci. Instrum.* 77 (2006) 053104.
- [20] B.W. Kempshall, L.A. Giannuzzi, B.I. Prenzler, F.A. Stevie, S.X. Da, Comparative evaluation of protective coatings and focused ion beam chemical vapor deposition processes, *Journal of Vacuum Science & Technology B: Microelectronics and Nanometer Structures* 20 (2002) 286–290.
- [21] S.-G. Hur, E.-T. Kim, J.-H. Lee, G.-H. Kim, S.-G. Yoon, Characterization of photoconductive CdS thin films prepared on glass substrates for photoconductive-sensor applications, *Journal of Vacuum Science & Technology B: Microelectronics and Nanometer Structures* 26 (2008) 1334–1337.
- [22] Y.H. Sun, Y.J. Ge, W.W. Li, D.J. Huang, F. Chen, L.Y. Shang, P.X. Yang, J.H. Chu, Structural and optical analysis of CdS thin films grown by magnetron sputtering technique, *Journal of Physics: Conference Series*, 276 (2011) 012187.
- [23] G. Liu, T. Schulmeyer, J. Brötz, A. Klein, W. Jaegermann, Interface properties and band alignment of $\text{Cu}_2\text{S}/\text{CdS}$ thin film solar cells, *Thin Solid Films* 431–432 (2003) 477–482.
- [24] J. Hernández-Borja, Y.V. Vorobiev, R. Ramírez-Bon, Thin film solar cells of CdS/PbS chemically deposited by an ammonia-free process, *Solar Energy Materials and Solar Cells* 95 (2011) 1882–1888.
- [25] J.J. Choi, W.N. Wenger, R.S. Hoffman, Y.-F. Lim, J. Luria, J. Jasieniak, J.A. Marohn, T. Hanrath, Solution-Processed Nanocrystal Quantum Dot Tandem Solar Cells, *Advanced Materials* 23 (2011) 3144–3148.
- [26] J.M. Luther, J. Gao, M.T. Lloyd, O.E. Semonin, M.C. Beard, A.J. Nozik, Stability assessment on a 3% bilayer PbS/ZnO quantum dot heterojunction solar cell, *Advanced Materials* 22 (2010) 3704–3707.
- [27] P.R. Brown, R.R. Lunt, N. Zhao, T.P. Osedach, D.D. Wanger, L.-Y. Chang, M. G. Bawendi, V. Bulovic, Improved current extraction from ZnO/PbS quantum dot heterojunction photovoltaics using a MoO_3 interfacial layer, *Nano Letters* 11 (2011) 2955–2961.

- [28] A.K. Rath, M. Bernechea, L. Martinez, G. Konstantatos, Solution-processed heterojunction solar cells based on p-type PbS quantum dots and n-type Bi₂S₃ nanocrystals, *Advanced Materials* 23 (2011) 3712–3717.
- [29] G. Zhai, A. Bezryadina, A.J. Breeze, D. Zhang, G.B. Alers, S.A. Carter, Air stability of TiO₂/PbS colloidal nanoparticle solar cells and its impact on power efficiency, *Applied Physics Letters* 99 (2011) 063512–063513.
- [30] L. Etgar, T. Moehl, S. Gabriel, S.G. Hickey, A. Eychmüller, M. Grätzel, Light energy conversion by mesoscopic PbS quantum dots/TiO₂ heterojunction solar cells, *ACS Nano* 6 (2012) 3092–3099.
- [31] L.-Y. Chang, R.R. Lunt, P.R. Brown, V. Bulović, M.G. Bawendi, Low-temperature solution-processed solar cells based on PbS colloidal quantum dot/CdS heterojunctions, *Nano Letters* 13 (2013) 994–999.
- [32] L.A.A. Pettersson, L.S. Roman, O. Inganäs, Modeling photocurrent action spectra of photovoltaic devices based on organic thin films, *Journal of Applied Physics* 86 (1999) 487–496.
- [33] M. Law, M.C. Beard, S. Choi, J.M. Luther, M.C. Hanna, A.J. Nozik, Determining the internal quantum efficiency of PbSe nanocrystal solar cells with the aid of an optical model, *Nano Letters* 8 (2008) 3904–3910.
- [34] L. Cademartiri, E. Montanari, G. Calestani, A. Migliori, A. Guagliardi, G.A. Ozin, Size-dependent extinction coefficients of PbS quantum dots, *Journal of the American Chemical Society* 128 (2006) 10337–10346.
- [35] I. Moreels, K. Lambert, D. Smeets, D. De Muynck, T. Nollet, J.C. Martins, F. Vanhaecke, A. Vantomme, C. Delerue, G. Allan, Z. Hens, Size-dependent optical properties of colloidal PbS quantum dots, *ACS Nano* 3 (2009) 3023–3030.
- [36] V. Plotnikov, Fabrication of ultra thin CdS/CdTe solar cells by magnetron sputtering, University of Toledo, 2009.
- [37] J. Tang, E.H. Sargent, Infrared colloidal quantum dots for photovoltaics: fundamentals and recent progress, *Advanced Materials* 23 (2011) 12–29.
- [38] G. Vigil, O.N.A. Arias-Carbajal, P. Mendoza, R. Rez, R. Santana, G. Guez, H. Sastre, J. Ndez, J.C. Alonso, G. Moreno, E.A.G. Contreras-Puente, A. Morales-Acevedo, Improving the efficiency of CdS/CdTe solar cells by varying the thiourea/CdCl₂ ratio in the CdS chemical bath, *Semiconductor Science and Technology* 20 (2005) 819–822.
- [39] J.L. Peña, O. Arés, V. Rejón, A. Rios-Flores, J.M. Camacho, N. Romeo, A. Bosio, A detailed study of the series resistance effect on CdS/CdTe solar cells with Cu/Mo back contact, *Thin Solid Films* 520 (2011) 680–683.
- [40] J. Tang, K.W. Kemp, S. Hoogland, K.S. Jeong, H. Liu, L. Levina, M. Furukawa, X. Wang, R. Debnath, D. Cha, K.W. Chou, A. Fischer, A. Amassian, J.B. Asbury, E. H. Sargent, Colloidal-quantum-dot photovoltaics using atomic-ligand passivation, *Nat Mater* 10 (2011) 765–771.